HHS Public Access

Author manuscript

Oncogene. Author manuscript; available in PMC 2020 September 18.

Published in final edited form as:

Oncogene. 2018 September ; 37(38): 5175–5190. doi:10.1038/s41388-018-0325-x.

Loss of *MAOA* in epithelia inhibits adenocarcinoma development, cell proliferation and cancer stem cells in prostate

Chun-Peng Liao[#1,2,3], **Tzu-Ping Lin**[#1,2,4], **Pei-Chuan Li**[#1,2], **Lauren A. Geary**[1,2], **Kevin Chen**[1,2], **Vijaya Pooja Vaikari**[1,2], **Jason Boyang Wu**[5], **Chi-Hung Lin**[4], **Mitchell E. Gross**[3,6], **Jean C. Shih**[1,2,6,7,8]

[1]Department of Pharmacology and Pharmaceutical Sciences, School of Pharmacy, University of Southern California, Los Angeles, CA 90089-9121, USA

[2]USC-Taiwan Center for Translation Research, University of Southern California, Los Angeles, CA 90089-9121, USA

[3]Lawrence J. Ellison Institute for Transformative Medicine, Keck School of Medicine, University of Southern California, Los Angeles, CA 90033-9075, USA

[4]Institute of Clinical Medicine, School of Medicine, National Yang-Ming University, Taipei, WA 11221, Taiwan

[5]Department of Pharmaceutical Sciences, College of Pharmacy, Washington State University, Spokane 99210-1495, USA

[6]Norris Comprehensive Cancer Center, Keck School of Medicine, University of Southern California, Los Angeles 90089-9176 CA, USA

[7]Department of Cell and Neurobiology, Keck School of Medicine, University of Southern California, Los Angeles, CA 90089-9037, USA

[8]College of Pharmacy, Taipei Medical University, Taipei 11031, Taiwan

[#] These authors contributed equally to this work.

Abstract

Monoamine oxidase A (MAOA) is a mitochondrial enzyme, which degrades monoamine neurotransmitters and dietary amines and produces H_2O_2. Recent studies have shown increased MAOA expression in prostate cancer (PCa), glioma, and classical Hodgkin lymphoma. However, the biological function of MAOA in cancer development remains unknown. In this study, we investigated the role of MAOA in the development of prostate adenocarcinoma by creating a prostate-specific *Pten/MAOA* knockout (KO) mouse model, in which *MAOA-floxP* mouse was crossed with the conditional *Pten* KO PCa mouse that develops invasive PCa. In contrast to *Pten* KO mice, age-matched *Pten/MAOA* KO mice exhibited a significant decrease in both prostate size and the incidence of invasive cancer. We observed a significant decline in AKT phosphorylation

[✉]Jean C. Shih jcshih@usc.edu.

Electronic supplementary material The online version of this article (https://doi.org/10.1038/s41388-018-0325-x) contains supplementary material, which is available to authorized users.

Conflict of interest The authors declare that they have no conflict of interest.

and Ki67 expression in *Pten/MAOA* KO mice, which reduced epithelial cell growth and proliferation. As cancer stem cells (CSCs) are required for tumor initiation and growth, we investigated expression of OCT4 and NANOG in the setting of decreased MAOA expression. We found that both OCT4 and NANOG were significantly attenuated in the prostate epithelia of *Pten/MAOA* KO mice compared to *Pten* KO mice, which was confirmed with targeted knockdown of MAOA with a short-hairpin(sh) vector targeting MAOA compared to cells transfected with a control vector. Expression of other markers associated with the a stem cell phenotype, including CD44, α2β1, and CD133 as well as HIF-1α^{+}CD44^{+} stem cells were all decreased in shMAOA PCa cells compared with empty vector-transfected control cells. We also found spheroid formation ability in PCa cells was decreased when endogenous MAOA was suppressed by siRNA or MAOA inhibitor clorgyline in a colony formation assay. Using the TCGA database, elevated MAOA expression was associated with reduced *Pten* levels in high Gleason grade in patient samples. Further, we found that *Pten*-positive PCa cells were more resistant to clorgyline treatments than *Pten*-null cells in tumorigenicity and stemness. Taken together, these studies suggest that MAOA expression promotes PCa development by increasing cell proliferation and CSCs and highlights the potential use of MAOA inhibitors for the treatment of PCa.

Introduction

Monoamine oxidase A (MAOA) is a mitochondrial enzyme, which degrades monoamine neurotransmitters, including serotonin and norepinephrine, via oxidative deamination and produce H_2O_2 [1]. The role of MAOA in aggression, depression, and autism has been well studied [2, 3]. Previous studies have shown elevated expression of MAOA in high-grade prostate cancer (PCa) with Gleason score 4 or 5, suggesting a novel role of MAOA in advanced PCa progression [4, 5]. Our recent study showed that MAOA promotes the proliferation, migration, and invasion of human and mouse PCa cells in vitro and the growth and metastasis of xenograft prostate tumors in vivo, mediated by convergent epithelial-mesenchymal transition (EMT), tumor hypoxia, and oxidative stress [6]. Further, a target-specific MAOA inhibitor was developed as a novel cancer therapeutic agent and non-invasive diagnostic tool for PCa [7] and glioma [8]. In addition, MAOA is also increased in classical Hodgkin lymphoma [9].

PCa is the second leading cause of cancer deaths in men in the United States [10]. PCa is a heterogeneous disease attributed to a variety of genetic and epigenetic alterations. The deletion and mutation of Phosphatase and tensin homolog (*Pten*) has been reported in 30% of primary and in more than 70% of advanced PCa patients [11]. Loss of PTEN function, leading to activation of the downstream PI3K/AKT and other regulatory pathways, is one of the most common genetic alterations in human PCa [12].

Transgenic mouse models with modified gene activation, expression, or deletion have been widely used to recapitulate human cancer progression in cancer research. Deletion of *Pten* in whole mice induces the death of embryos; hence, the mouse model with ARR2PB-Cre-mediated *Pten* deletion specifically in prostatic epithelia has been developed to mimic human disease pathogenesis toward prostate adenocarcinoma [13, 14]. In this conditional *Pten* knockout (KO) model, the male mouse loses *Pten* expression specifically in prostate

epithelia and develops hyperplasia, which progresses to cellular atypia and murine prostatic intracellular neoplasia (PIN) at 2 months of age and finally adenocarcinoma at 3–6 months of age. This mouse model is one of the few capable of developing castration-resistant PCa in a low-androgen environment after castration. It has been widely used to evaluate the in vivo functions of a variety of genes that participate in PCa development. By combining with other loxP models such as GRP78 [15] or survivin [16], recent studies have shown the efficiency of ARR2PB-Cre in inactivating *Pten* and associated target genes in prostate epithelium. Thus, this model provides an applicable and useful in vivo platform for studying the role of MAOA in PCa.

The human *MAOA* gene consists of 15 exons where exon 12 encodes the flavin adenine dinucleotide cofactor-binding site, which is responsible for the catalytic activity [17, 18]. The floxed-MAOA mouse model was generated by inserting the loxP sequence in intron 11 and intron 12, which flank exon 12 [19]. When this mouse model was combined with CMV-Cre mice, which ubiquitously express Cre recombinase, no MAOA activity was detected in tissues examined due to a pronounced reduction in the functional transcription [19], indicating that the deletion of exon 12 can efficiently inactivate MAOA in tissues.

To understand the roles of MAOA in prostate tumorigenesis, we studied the effects of crossing the *Pten* KO mice with a *MAOA* KO strain to produce targeted KO of both genes in prostate tissue. Here we report the generation of *Pten/MAOA* KO mice and the characterization of the effects of MAOA deletion on spontaneous development of *Pten* KO prostate tumors using this unique double-KO mouse model.

Results

Generation of prostate epithelial-specific *MAOA* KO and *Pten/MAoA* KO mice

Male mice carrying *Pten*-loxP gene and the *ARR$_2$PB*-promoter-driven *PB-Cre4* transgene, which were previously described [13, 14], were crossed with female homozygous floxed-*MAOA* gene in which exon 12 is flanking by loxP sequences [19] (Fig. 1a). This cross yielded both the prostate-specific *MAOA* KO with intact and functional *Pten* alleles, and *Pten/MAOA* KO with both *Pten* and *MAOA* genes deficient in prostate epithelium. The genotype of each offspring was determined by PCR as described in Materials and methods. The PCR primer locations and the size of PCR products of Cre and *MAOA* are presented in Fig. 1b. Genomic DNA collected from tails and prostates of mice encoding ARR2PB-Cre (*MAOA* KO, *Pten* KO, and *Pten/MAOA* KO) was detectable with a 0.5-kb band when using Cre primers in PCR (Fig. 1c, upper panel). When using the *MAOA* primer set for genotyping PCR, the wild-type *MAOA* (1.2 kb) band was detectable in tail and prostate (anterior prostate (AP), ventral prostate (VP), and dorsal–lateral prostate (DLP)) genomic DNA samples isolated from *Pten* KO tissues. In contrast, the floxed-*MAOA*, which contains two loxP sequences and is determined by a 1.5 kb DNA fragment in PCR using the *MAOA* primer set, was detectable from the tail or prostate genomic DNA samples from wild-type mice. These mice carried the floxed-*MAOA* gene but without the ARR2PB-Cre allele, so there was no detectable DNA recombination in floxed-*MAOA* alleles in these prostate epithelium. However, in *MAOA* KO and in *Pten/MAOA* KO, the floxed-*MAOA* gene was detectable only in tails. Instead, the KO-*MAOA* gene (determined by a 0.6 kb band in PCR

using the MAOA primer set) was detected in AP, VP, and DLP of these two genotypes (Fig. 1c, lower panel). Thus, all four genotypes, *MAOA* KO, *Pten* KO, *Pent/MAOA* KO, and wild-type mouse models were obtained and confirmed.

Prostate-specific *MAOA* deletion inhibits prostate tumorigenesis

We first investigated whether *MAOA* deletion may affect the development of normal prostate epithelium. As shown in Fig. 2, prostates dissected from 4-month-old *MAOA* KO and wild-type mice showed similar anatomic morphology and size in both ventral (Fig. 2a) and dorsal views (Fig. 2b), including bladder, seminal vesicle, AP lobes, VP lobes, and DLP lobes. Prostate lobes of both wild type and *MAOA* KO showed soft and transparent tissues, and no gross tumors nor abnormal blood vessels, often seen in cancer. Similar morphology was observed in 6-month-old wild-type and *MAOA* KO mice (Fig. 2a, b, lower panels). Histologic analysis of prostatic tissue sections of DLP (Fig. 2c), VP, and AP (Fig. S1) from 4- and 6-month *MAOA* KO demonstrated similar glandular morphology with age-matched wild-type controls, including double-epithelial cell layers with intact basement membranes surrounding prostate glands and a small number of stroma cells. Importantly, neither atypical nor invasive epithelial cells were detectable in *MAOA* KO.

We then compared the prostate morphology between *Pten* KO and *Pten/MAOA* KO to investigate the effect of MAOA on PCa development. As shown in Fig. 2, prostates from either 4- or 6-month-old *Pten* KO had enlarged APs and VPs in the ventral view (Fig. 2a) and DLPs in the dorsal view compared to wild-type or *MAOA* KO mice (Fig. 2b). These prostate lobes had opaque white and yellow tumors as well as atypical, dilated blood vessels (indicated by red arrows). Moreover, prostates from *Pten/MAOA* KO at 6 months were larger than that at 4 months. Notably, APs were usually fused to the adjacent seminal vesicle, indicative of local invasion, in 6-month-old *Pten* KO prostates. However, in comparing *Pten/MAOA* KO with *Pten* KO prostate lobes isolated at either 4 or 6 months, *Pten/MAOA* KO (shown in Fig. 2a, b) were smaller in size, but still larger than wild type or *MAOA* KO. Yellow tumors were also observed in all prostate lobes. However, no atypical blood vessel formation was observed and portions of the lobes were still soft and transparent in *Pten/MAOA* KO mice.

Histological comparison of hematoxylin and eosin (H&E)-stained tissues from both *Pten* KO and *Pten/MAOA* KO is shown in Fig. 3a. Typical adenocarcinoma was detected in all three lobes of the 4-month-old *Pten* KO ($n = 4$) animals, identified as multiple layers of epithelial cells with open chromatin pattern, high stromal cell density, angiogenesis with atypical blood vessels (as indicated by red arrows), and focal areas of basement membrane invasion (as indicated by black arrows). In 6-month-old *Pten* KO mice ($n = 3$), a more aggressive pattern of cancer growth was observed. Specifically, the basement membrane of prostate glands was almost completely eroded and replaced with invasive cancer epithelial cells, with prominent nucleoli, extending into adjacent stroma. Angiogenesis with blood vessel formation was also found in adjacent stroma (as indicated by red arrows). However, no adenocarcinoma was observed in any of the *Pten/MAOA* KO mice (4 mice in 4-month group; 5 mice in 6-month group). Instead, only the PIN morphology was seen with

disordered layers of epithelial cells in prostate glands confined within a basement membrane, surrounded by myoepithelial cell layers (Fig. 3a and Fig. S1).

Next, PTEN and MAOA expression in tissue sections was evaluated. We performed immunohistochemistry (IHC) staining on prostate tissue sections isolated from 6-month-old DLP of each genotype. Minimal PTEN expression was found in epithelia in both *Pten* KO and *Pten/MAOA* KO. As expected, PTEN-positive epithelial cells were detectable in both wild type and *MAOA* KO. Further, PTEN-positive stromal cells were detectable in all genotypes, confirming that *Pten* deletion was specific to epithelial cells (Fig. 3b). Minimal MAOA staining was seen in *MAOA* KO and *Pten/MAOA* KO mice; as expected, MAOA expression was positive in wild type and *Pten* KO (Fig. 3c).

We also investigated if *MAOA* deletion alters the distribution of luminal and basal cells by performing CK8 (a luminal cell marker)- and p63 (a basal cell marker)-based IHC staining on prostate tissue sections of all four genotypes. CK8-positive cells were detected in epithelia of all genotypes (Fig. S2A), and p63-positive cells were located in the basal cell layer close to the basement membrane in all four genotypes (Fig. S2B). These results suggest that *MAOA* deletion did not alter the distribution and location of luminal and basal cells during tumorigenesis.

The incidence of PIN and adenocarcinoma in prostate lobes in all four genotypes at these two age groups is summarized in Fig. 4. At 4 and 6 months, adenocarcinoma was observed in all *Pten* KO prostate lobes while normal morphology was observed in all wild type and *MAOA* KO prostate lobes. In contrast, PIN was observed in nearly all *Pten/MAOA* KO at both 4 and 6 months, except one area of adenocarcinoma in the VP at 6 months of age (Fig. 4a, b). PCa incidence was also calculated in aggregate (Fig. 4c). As each prostate can be divided into three lobes (anterior, dorsal, and dorsolateral), we compared the incidence of adenocarcinoma in *Pten* KO and *Pten/MAOA* KO mice aggregating across all lobes at 4 and 6 months. Figure 4c shows adenocarcinoma decreased from 100% in *Pten* KO ($n = 4$ for each age) to 0% (4 months/$n = 4$) and 7% (6 months/$n = 5$) in *Pten/MAOA* KO. Thus, loss of *MAOA* expression in murine *Pten*-null prostate epithelia efficiently keeps prostates in the PIN stage and reduces prostate tumorigenesis.

Loss of *MAOA* inhibits AKT phosphorylation and cell proliferation in prostate epithelium

It is known that PTEN deletion promotes phosphorylation of AKT, a well-established tumor-promoting factor, which increases cell proliferation and migration in PCa [14, 20]. Interestingly, our recent studies in PCa cell line models suggest that MAOA stimulates cell proliferation through the AKT/FOXO1/TWIST1 pathway [6]. Thus, we examined if *MAOA* deletion altered AKT phosphorylation in PCa development. Prostate sections collected from 6-month-old mice were stained for p-AKT expression. p-AKT was detected at considerably higher levels in the epithelium of *Pten* KO compared with the *Pten/MAOA* KO model (Fig. 5a). p-AKT-positive cells were significantly decreased in *Pten/MAOA* KO compared to *Pten* KO mice (96.18 ± 1.5% vs 33.57 ± 5.0%; Fig. 5b). Our results indicate that *MAOA* deletion suppresses AKT phosphorylation induced by *Pten* deletion in prostate epithelial cells, suggesting the role of MAOA in AKT pathways in PCa development.

Next, we detected Ki67 (a proliferative cell marker) and apoptosis markers in cells on tissue sections from DLP of 6-month-old *Pten* KO and *Pten/MAOA* KO mice. Ki67-positive cells were all located in the epithelial area in both genotypes (Fig. 5c). Using the ImmunoRatio software [21], we found $Ki67^+$ epithelial cells were significantly decreased in *Pten/MAOA* KO compared to *Pten* KO mice (5.57% vs 9.97%; Fig. 5d). In examining apoptosis markers, only a small fraction of cleaved caspase-3-labeled cells were detectable in both genotypes (specifically, 1.08% in *Pten* KO compared to 3.16% in *Pten/MAOA* KO, which did not show significant difference; Fig. 5e, f), and no caspase 9-, p53-, or BCL-2-positive cells were detected in these two genotypes (Fig. S3). These data suggest MAOA promotes proliferation rather than apoptosis of PCa cells.

Loss of MAOA reduces stem cell subpopulation in prostates and further prohibits cancer development

Recently, studies in cancer stem cells (CSCs) have showed that elevated PI3K/AKT signaling in CSCs promotes the viability of such cell populations in PCa [22] and colon cancer [23]. Since MAOA deletion attenuated tumor progression as well as AKT phosphorylation in this PCa model, we investigated if characteristics associated with CSCs were also altered in the setting of MAOA deletion. CSCs are commonly found in many solid cancers [24], including prostate [25], and are associated with tumor formation, cancer metastasis, and drug resistance [26, 27]. IHC staining was performed using antibody against mouse OCT4 on prostate tissue sections from 6-month-old *Pten* KO and *Pten/MAOA* KO mice. The percentage of OCT4-positive cells in epithelia was 43.7–60.1% in three *Pten* KO prostate lobes (AP, VP, and DLP) compared to 15.7–18.5% in *Pten/MAOA* KO prostate lobes (Fig. 6a, b). NANOG is another important CSC marker, which binds to OCT4 to form a functional complex to activate downstream stemness pathways in stem cells [28]. We investigated the distribution of NANOG-expressing cells. $NANOG^+$ cells in epithelia was 35.5–52.9% in *Pten* KO and 9.3–15.5% in *Pten/MAOA* KO (Fig. 6c, d). Interestingly, most $OCT4^+$ or $NANOG^+$ cells detected in these two genotypes were found in luminal positions in epithelia, which were also positive for CK8 expression (Fig. S2A), suggesting that many luminal cells also express stemness markers.

MAOA regulates CSC characteristics in PCa cells

To confirm our IHC data obtained from mouse models, the interaction between MAOA and stem cell genes was investigated using the human PCa LNCaP cell line. LNCaP cells are negative for PTEN expression due to a deletion in one *Pten* allele and a mutation in the other allele [29]. Thus, knockdown of *MAOA* in this human cell line will mimic the *Pten/MAOA* KO mice. Our results showed that stable knockdown of *MAOA* in LNCaP cells reduced *MAOA* mRNA level as expected (Fig. 7a). Interestingly, it also reduced *Oct4* and *Nanog* mRNA levels (Fig. 7a). Next, we examined the stem cell populations in both cell lines using flow cytometry by staining LNCaP-shControl and -shMAOA cells with phycoerythrin (PE)- or fluorescein isothyocianate (FITC)-conjugated antibodies against CD44, $\alpha 2\beta 1$, and CD133 [25]. Our results showed that the $CD44^+$, $\alpha 2\beta 1^+$, and $CD133^+$ stem cell population sizes in MAOA knockdown LNCaP cells were only 26.0 ± 7.5%, 52.7 ± 7.8%, and 23.1 ± 5.4% (Fig. 7b–d), as compared to the control cells (as 100%), respectively. In addition, shMAOA also decreases the proliferation of CSCs. As compared to LNCaP-shControl,

$Ki67^+CD44^+$ and $Ki67^+CD133^+$ stem cell populations were reduced to 24.5 ± 17.9% (Fig. 7e) and 57.3 ± 15.9% (Fig. 7f), respectively, in LNCaP-shMAOA. These results suggest that MAOA promotes CSC proliferation in PCa.

Recent studies have shown hypoxia-inducible factor 1-alpha (HIF-1α) promotes stem cell proliferation in cancer cells [30, 31] and our previous report demonstrates that MAOA associates with HIF-1α in PCa tumorigenesis [6]. Thus, to investigate the interactions between MAOA and HIF-1α in regulations of sternness in PCA, we determine HIF-1α $^+CD44^+$ stem cells in shMAOA and shControl PCa cells under hypoxia condition by flow cytometry. Interestingly, this stem cell population was significantly reduced in LNCaP-shMAOA (73.6 ± 12.0%) and 22RV1-shMAOA (64.5 ± 18.9%) as compared to shControl cells (Fig. 7g, h). These results suggest that MAOA may stimulate stemness through HIF-1α in PCa.

The spheroid-forming assay has been widely used to mark the CSC phenotype. To determine the role of MAOA in PCa CSCs, LNCaP cells were seeded and cultured in three-dimensional spheroid-forming analysis. After 12 days culturing in Matrigel, LNCaP-shMAOA spheroids were significantly decreased compared to those formed from LNCaP-control cells. We observed both a decrease in average spheroid size (LNCaP-shMAOA: 63.4 ± 10.9 μm vs LNCaP-control: 112.0 ± 15.8 μm) and number (LNCaP-shMAOA: 32.7 ± 3.8 colonies/well vs LNCaP-control: 88.6 ± 8.3 colonies/well) in the LNCaP-shMAOA cells compared to controls (Fig. 8a–c). These results were further explored by using the MAOA inhibitor, clorgyline, in PCa cell lines. Figure 8d, e shows that LNCaP spheroid number significantly decreased in a concentration-dependent manner. Similar results were also obtained using 22RV1 with either shRNA transformations or clorgyline treatments (data not shown). These in vivo and in vitro findings suggest that inhibition of *MAOA* activity diminishes the prostate CSC populations, indicating the role of MAOA in promoting stemness in PCa.

Interaction of MAOA and *Pten* in PCa progression

It is well-known that reduced *Pten* expression in cancer will lead to poor prognosis. Here we investigated the interaction of MAOA and *Pten* expressions in clinical data. Two TCGA datasets [32, 33] with patient-specific annotations, including Gleason score were used. Pathologic Gleason grade is a critical pathologic factor used in prognostication and treatment planning for patients with newly diagnosed PCa [34]. Interrogation of these TCGA dataset revealed that elevated MAOA expression is associated with low *Pten* expressions in patient groups with Gleason scores 7 and above (Fig. 9a, b).

The effect of *Pten* on clorgyline inhibition of tumorigenesis

Two PCa cell lines with (22RV1) or without (LNCaP) Pten expression were used in two-dimensional (2D) colony formation and MTT surviving assay for testing stemness and tumorigenesis. Both cell lines showed a dose-dependent reduction in colony forming ability with more colonies observed in 22RV1 than LNCaP cells treated with the same clorgyline concentration. As compared to untreated controls, the colony number was 83% (1 μm) and 76% (10 μm) in 22RV1, and this number decreased to only 64% (1 μm) and 33% (10 μm) in

LNCaP (Fig. 10a, b). In a MTT survival assay, again, 22RV1 was less responsive to clorgyline than LNCaP. While the cell viability rate was 91% in 22RV1 as compared to untreated controls at the concentration of 10 μm, cell viability was reduced to 76% in LNCaP (Fig. 10c). Taken together, the clinical and in vitro results suggest that MAOA's regulation of tumorigenesis in PCa is associated with *Pten* status.

Discussion

In this study, we investigated the role of MAOA in PCa development and in the initiation of PCa using *Pten* KO mouse models, which share a similar genetic defect with human PCa patients. We knocked down *MAOA* expression specifically in prostate by introducing the *MAOA*-floxP allele into a conditional *Pten*-null PCa mouse model. *MAOA* deletion did not affect prostate morphology compared to wild-type mice (Fig. 2a, b), while KO of *MAOA* significantly reduced cancer formation and epithelial cell proliferation in *Pten*-null mice. Compared to the 100% incidence of tumors in *Pten* KO mice at 6 months, only 1 out of 15 lobes examined in 5 *Pten/MAOA* KO mice (3 lobes in each mouse) developed PCa (Fig. 4b). We note that most of the adenocarcinoma developed in the VP lobe, which is known to contain large acini lined with cuboidal epithelial cells further coupled with a flat mucosal layer and a thin stromal cell line. When anatomy has been compared between mouse and human prostate on a per lobe basis, tumors are generally observed in the DLP lobe as most similar to the peripheral zone in human PCa [35]. These studies in aggregate indicate a profound role of MAOA in determining the initiation and development prostate tumors in a spontaneous mouse PCa model. Although we draw this conclusion solely by using *Pten* KO model, our study merits future investigation by extending the use of other transgenic mouse models available for PCa research.

In contrast to the parental *Pten* KO mice, most *Pten/MAOA* KO mice showed PIN but no signs of PCa (Figs. 2 and 3), indicating the effectiveness of MAOA abrogation in PCa development initiated by PTEN loss. Of note, unlike *Pten* KO prostates, the prostate glands in *Pten/MAOA* KO mice were all surrounded by intact basement membranes, with no epithelial cells invading into adjacent stromal areas (Fig. 3a and Fig. S1), which represents a significant reduction in malignancy caused by MAOA inactivation. *Pten* deletion in mouse prostates always instigates PIN first, a default step prior to the development of adenocarcinoma, as evidenced by our prior studies [14, 36]. Hence, *MAOA* KO is unable to prevent PIN development initiated by *Pten* deletion in epithelial cells, suggesting that MAOA may not be responsible for the PIN formation but rather the control of switch from PIN to PCa. Collectively, our observations in the *Pten/MAOA* KO model clearly reveal the important roles of MAOA in each stage of PTEN-dependent spontaneous prostate tumorigenesis.

PTEN regulates cell proliferation mainly through the PI3K-AKT-p27 pathway [37], with *Pten* loss resulting in elevated AKT phosphorylation and robust prostatic tumorigenesis in mice [14]. We observed downregulation of AKT phosphorylation in *Pten*-null prostatic epithelia when MAOA deletion was introduced (Fig. 5a, b), which suggests that *MAOA* may stimulate abnormal cell proliferation in PCa through upregulation of AKT activity. This phenomenon is consistent with our previous observations made in human PCa cells, where

genetic knockdown of MAOA decreased the phosphorylation of AKT and other AKT-downstream factors such as FOXO1 [6]. Interestingly, we also found induced expression and activity of MAOA in both *Pten* KO primary prostate tumors and PTEN-knockdown human 22RV1 (wild-type PTEN) PCa cells [6]. These results suggest a reciprocal regulatory pattern between MAOA and PTEN, forming a "vicious cycle" to drive PCa progression, which lays mechanistic foundations for better disease control by untangling MAOA and PTEN [6]. This hypothesis is supported by evidence provided in this report. Analysis of two datasets within TCGA show elevated MAOA expression is associated with decreased *Pten* expression in PCa patients with high Gleason scores. Futhermore, similar effects were seen on stemness and cell viability in using the 22RV1 (*Pten*-positive) and LNCaP (*Pten*-negative) human PCa cell lines (Fig. 10). PTEN is one of the most commonly deleted/mutated tumor suppressor genes in human PCa, with PTEN loss observed in up to 70% of human PCa patients and correlated with an overall poor prognosis, and even subtle variations in PTEN dose have been shown to determine cancer susceptibility [11, 38]. Currently, a number of inhibitors against PI3Ks and AKT, both of which are direct PTEN-downstream target molecules, are undergoing clinical trial for different types of cancers, including PCa. Our studies thus provide a rationale to target MAOA to supplement PTEN-based therapy for potential synergistic treatment effects—especially, for the PCa subtype with aberrant PTEN status.

CSCs are critical in the initiation of PCa as well as progression to castration resistance [39]. According to the CSC hypothesis, cancer cells can be characterized as terminal-differentiated (TD) cells, transient-amplifying (TA) cells, and CSCs [40, 41]. Among these types, CSCs are the only cell type with unlimited proliferative potential and plasticity, which allow CSCs to escape therapies [42]. It is known that the CSC populations isolated from the *Pten* KO model are able to regenerate PCa in vitro and in vivo [43–45], and the generation of CSC may be through TD cell reprograming/de-differentiation [43]. Conflicting studies have concluded that CSCs arise from either the basal or luminal compartments [46–48]. In this study, we found that most $OCT4^+$ and $NANOG^+$ PCa cells in *Pten* KO mice were located in luminal cell areas (demarcated by CK8 positivity) compared with less $OCT4^+$ and $NANOG^+$ cells detected in similar areas in the *Pten/MAOA* KO mice (Fig. 6a, c). These contrasting observations suggest that *MAOA* may stimulate expression of stemness genes in luminal cells, resulting in subsequent de-differentiation or reprograming in TD cells and, later, the formation of CSCs.

Our study provides evidence that *MAOA* influences the formation of CSCs in PCa. Previously, Xu et al. has demonstrated in vitro that inhibition of both survivin and MAOA in PCa cell lines results in reduced cell growth and migration [49], suggesting a role of MAOA in PCa tumorigenesis. Here we further show that CSC populations as well as stemness marker expression were significantly reduced in *Pten/MAOA* KO mice (Fig. 6) and in LNCaP-shMAOA cells (Fig. 7) compared to their respective controls. Targeted knockdown or inhibition of MAOA, with either siRNA or clorgyline treatments, respectively, in LNCaP cells dramatically decreased the size and number of spheroids formed (Fig. 8), suggesting that MAOA is important in CSC regulation. Therefore, it would be of interest to consider mechanisms connecting MAOA expression and function with CSC populations in PCa. One possible mediator for this effect involves HIF-1α, a transcription factor and master regulator of hypoxia. We previously demonstrated that elevated MAOA expression promotes HIF-1α/

VEGF-A/AKT signaling pathways, which results in increased EMT marker expression in PCa cell lines and xenografts [6]. The finding is consistent with the results of studies centering on hypoxia in cancer, which showed that HIF-1α is able to stimulate stem cell proliferation in normal somatic and cancer cells [30, 31]. This hypothesis is also supported by our findings that *Pten/MAOA* KO prostates were harboring less percentage of p-AKT-expressing epithelial cells as compared to *Pten* KO counterparts (Fig. 5a, b). MAOA knockdown cells also present less-proliferative CSCs ($Ki67^+CD44^+$ or $Ki67^+CD44^+$; Fig. 7e, f) and HIF-1α-positive CSCs as compared to controls (Fig 7g, h). Collectively, these studies suggest that MAOA may maintain and/or promote CSC populations through HIF-1α pathways in PCa. Nevertheless, our work does not rule out the existence of other factors, which may work alone or together with HIF-1α in regulation of stemness in PCa.

In summary, our data show the functional role of *MAOA* in the initiation and progression of PCa in a spontaneous PCa mouse model, which provides a basis for targeting MAOA activity in PCa patients. Future investigations are planned to address *MAOA*-regulated pathways in PCa, especially those associated with dysfunction of PTEN as well as the mechanistic connection between *MAOA* and CSC subpopulation in PCa. This newly developed *Pten/MAOA* KO mouse model and the parental *Pten* KO mouse may serve as useful in vivo research tools for future PCa studies.

Materials and methods

Animals

For generations of *MAOA* KO and *Pten/MAOA* KO, we used floxed-*MAOA* allelic ($A^{f/f}$) female mice on a 129/SvEvTac6 background [19] and bred with male mice carrying ARR2PB-Cre and floxed *Pten* ($Pten^{f/f}$) alleles on C54BL/6xDBA2/129 background [14]. Animals were housed and maintained under identical conditions and animal experimentation was conducted in accordance with the ethical federal guidelines mandated by the University of Southern California Institutional Animal Care and Use Committee.

Mouse genotyping

Genomic DNA from mouse tail was lysed using the quick genotyping kit (Bioland Scientific). In brief, tail snips were collected into microtubes followed by addition of lysis buffer for each sample. Samples were subjected to heat at 95 °C for 10 min and then gradual cooling to 4 °C. Subsequently, DNA-stabilizing buffer was added to each sample with gentle mix. The final preparation was directly used for each PCR reaction. To validate the tissue-specific deletion of *Pten* and *MAOA* in mouse prostates, 5 mg prostate tissue was harvested from mice at the time of sacrifice and used to extract genomic DNA using QIAamp® DNA Mini kit (Qiagen) following the manufacturer's protocol. PCR primers, reaction conditions, and expected sizes of PCR products for genotyping are summarized in Table 1.

Histopathology

Prostate tissues collected from each mouse at different age categories were incubated in unbuffered zinc formalin solution (Thermo Fisher Scientific) at 4 °C overnight and then washed thrice in PBS and once in ethanol for 10 min before stored in 70% ethanol. Fixed

tissues were then processed by standard procedures, embedded in paraffin, cut to 5-μm sections onto glass microscope slides, and stained with hematoxylin and eosin (H&E) after deparaffinization and rehydration.

IHC analysis

Paraffinized prostate tissue sections were deparaffinized and rehydrated before being subjected to antigen retrieval in 10 mM sodium citrate buffer at 95 °C. Slides were then incubated in 1% H_2O_2 in methanol to block endogenous peroxidase activity. Sections were blocked with 10% normal goat serum (Vector Laboratories) and 0.3% Triton X-100 in Tris-buffered saline (TBS) for 1 h at room temperature and incubated in primary antibody working solutions at 4 °C overnight [44]. Antibodies and concentrations used in working solutions: PTEN, 1:400 and p-AKT, 1:500 (Cell Signaling Technology, Beverly, MA); MAOA, 1:400 (Santa Cruz Biotechnology); Ki67, 1:50 (Thermo Fisher Scientific); p63, 1:100 (Abcam, Cambridge); cytokeratin (CK) 8, 1:50 (Developmental Studies Hybridoma Bank); OCT4, 1:400 (Abcam); Caspase 9, 1:500 (Cell Signaling Technology); p53, 1:250 (Cell Signaling Technology); BCL-2, 1:500 (Santa Cruz Biotechnology); and NANOG, 1:400 (Abcam). To detect specific staining, sections were treated with the VECTASTAIN Elite ABC kit (Vector Laboratories) and the biotinylated secondary antibodies (Vector Laboratories). After washing with TBS, specific stains were developed with DAB+ (Dako). Digital images were captured using a Leica bright-field microscope and Spot Advanced software (Spot Imaging Solutions). To obtain quantitative IHC results, three fields were randomly chosen from each section. In each field, positive IHC-stained epithelial cells were counted and divided by the total number of epithelial cells. The total number of epithelial cells were taken as 100%. A minimum of three mice were used in each group.

Cell culture

Human PCa LNCaP and 22RV1 cells obtained from American Type Culture Collection were cultured in RPMI 1640 medium supplemented with 10% fetal bovine serum (FBS) and 1% antibiotics [6], with medium replaced every 3 days. PCa cells stably expressing either a scrambled shRNA (shControl) or a *MAOA*-targeting shRNA (shMAOA) were maintained with addition of puromycin (2 μg/ml) in culture medium.

Reverse transcription-quantitative PCR

Total cellular RNA, extracted by Direct-Zol RNA mini-prep kit (Zymo Research), was reverse transcribed to cDNA by Superscript III Kit (Thermo Scientific). The reaction product of reverse transcription was then subjected to PCR amplification using quantitative PCR (qPCR) master mix kit (Bioland). PCR signals were recorded and analyzed by iCycler (Bio-Rad). Sequences of primers used for qPCR are as follows: *MAOA*-F 5′-CAGTGGCAGGGTTTCCAG-3′, *MAOA*-R 5′-CACGGTCAGGCTGTTCTCG-3′; *OCT4*-F 5′-CCACATCGGCCTGTGTATATC-3′, *OCT4*-R 5′-AGCAAAACCCGGAGGAGT-3′; *NANOG*-F 5′-AAGTGGGTTGTTTGCCTTTG-3′, *NANOG*-R 5′-ATGCCTCACACGGAGACTGT-3′; and *18S rRNA*-F 5′-CGCCGCTAGAGGTGAAATTC-3′, *18S rRNA*-R 5′-CGAACCTCCGACTTTCGTTC-3′. A relative gene-expression quantification method was used to calculate the fold change of

mRNA expression according to the comparative Ct method using *18S rRNA* as an internal control for normalization.

Flow cytometry

Cultured cells were resuspended in Cell Staining Buffer (Biolegend) for 10 min on ice for blocking, following by staining with fluorescent-labeled antibodies in room temperature for 20 min. Stained cells were examined using BD LSR II Flow Cytometer (BD Biosciences) with FlowJo software. Antibodies used are FITC-conjugated human CD44 antibody (1 μg/1 × 10^6 cells, Biolegend), FITC-conjugated human α2β1 antibody (1 μg/1 × 10^6 cells, Biolegend), PE-conjugated human CD133/1 (AC133, 0.5 μg/1 × 10^6 cells, Miltenyli Biotec), and FITC-conjugated human Ki67 antibody (1 μg/1 × 10^6 cells, Biolegend).

Spheroid formation

The basic method was modified from our previous report [43]. Briefly, 500 human PCa cells were suspended with ice-cold 50% Matrigel (BD Bioscience)/RPMI 1640 (1% FBS) in a total volume of 500 μl. This mixture was then overlaid into a 24-well plate, supplied with 1 ml RPMI 1640 (1% FBS), and cultured at 37 °C for 10 days. Spheroids formed from cells were examined and photographed using a phase contrast microscope. Spheroid size was measured using ImageJ. For 2D colony formation, 500 human PCa cells were seeded in 96 wells and treated with clorgyline and cultured at 37 °C for 21 days.

Hypoxia culture

Five million PCa cells are cultured in EZ anaerobe gasgenerating pouch system with indicator (BD GasPak) at 37 °C as the description in manual. After 24 h, cells are stained with antibodies against HIF-1α (1 μg/1 × 10^6 cells, Biolegend), CD44, or CD133, and determined by flow cytometry.

MTT assay

PCa cells seeded in 96-well plates (5000 cells/well) are cultured with clorgyline at 37 °C for 96 h. The culture medium in each well is aspirated and replaced with 100 μl of MTT at the concentration of 0.5 mg/ml (Thiazolyl Blue Tetazolium, Sigma), incubated at 37 °C for 4 h, and then replaced again with dimethylsulfoxide (100 μl). The colorimetric intensity of formazan is quantified using an enzyme-linked immunosorbent assay reader at 590 nm. The percentage of cell viability is calculated according to the values of the control group as 100%.

Statistical analysis

All experimental results were repeated a minimum of three times (independent replicates) and are presented as means ± SD or means ± SEM. Statistical calculations were done with Microsoft Excel analysis tools. Differences between individual groups were analyzed by paired *t* test. *P* values < 0.05 were considered statistically significant.

Significance statement

Increased MAOA expression has been shown in clinically aggressive forms of PCa, glioma, and classical Hodgkin lymphoma. However, the biological mechanisms of MAOA in cancer development are not clear. In this study, we demonstrate that deletion of *MAOA* gene in prostate epithelia decreases the incidence of cancer, cell proliferation, and CSCs in *Pten* KO murine PCa model. Similar findings were shown in human PCa cell lines. These studies suggest that MAOA expression increases epithelial proliferation and CSCs. Taken together, this work demonstrates the role of MAOA in cancer development, highlighting the potential use of MAOA inhibitors for the treatment of PCa.

Supplementary Material

Refer to Web version on PubMed Central for supplementary material.

Acknowledgements

We would like to thank Dr. Pradip Roy-Burman for providing the conditional *Pten* deletion mouse model and for helpful technical discussions, Bin Qian (Department of Pharmacology and Pharmaceutical Sciences, University of Southern California) for technical assistance, F. Hong for critically reading the manuscript, and all members of the Jean C. Shih Laboratory and the Center for Apply Molecular Medicine at USC for assistance in various aspects of this work.

Funding This work was supported by the Department of Defense Prostate Cancer Research Program grant W81XWH-12-1-0282, the Daniel Tsai Family Fund, and the Boyd and Elsie Welin Professorship (to JCS). The content is solely the responsibility of the authors and does not necessarily represent the official views of the Department of Defense or other funding agency.

References

1. Shih JC, Chen K, Ridd MJ. Monoamine oxidase: from genes to behavior. Annu Rev Neurosci. 1999;22:197–217. [PubMed: 10202537]
2. Singh C, Bortolato M, Bali N, Godar SC, Scott AL, Chen K, et al. Cognitive abnormalities and hippocampal alterations in monoamine oxidase A and B knockout mice. Proc Natl Acad Sci USA. 2013;110:12816–21. [PubMed: 23858446]
3. Bach AW, Lan NC, Johnson DL, Abell CW, Bembenek ME, Kwan SW, et al. cDNA cloning of human liver monoamine oxidase A and B: molecular basis of differences in enzymatic properties. Proc Natl Acad Sci USA. 1988;85:4934–8. [PubMed: 3387449]
4. True L, Coleman I, Hawley S, Huang CY, Gifford D, Coleman R, et al. A molecular correlate to the Gleason grading system for prostate adenocarcinoma. Proc Natl Acad Sci USA. 2006;103:10991–6. [PubMed: 16829574]
5. Peehl DM, Coram M, Khine H, Reese S, Nolley R, Zhao H. The significance of monoamine oxidase-A expression in high grade prostate cancer. J Urol. 2008;180:2206–11. [PubMed: 18804811]
6. Wu JB, Shao C, Li X, Li Q, Hu P, Shi C, et al. Monoamine oxidase A mediates prostate tumorigenesis and cancer metastasis. J Clin Investig. 2014;124:2891–908. [PubMed: 24865426]
7. Wu JB, Lin TP, Gallagher JD, Kushal S, Chung LW, Zhau HE, et al. Monoamine oxidase A inhibitor-near-infrared dye conjugate reduces prostate tumor growth. J Am Chem Soc. 2015;137:2366–74. [PubMed: 25585152]
8. Kushal S, Wang W, Vaikari VP, Kota R, Chen K, Yeh TS, et al. Monoamine oxidase A (MAO A) inhibitors decrease glioma progression. Oncotarget. 2016;7:13842–53. [PubMed: 26871599]
9. Li PC, Siddiqi IN, Mottok A, Loo EY, Wu CH, Cozen W, et al. Monoamine oxidase A is highly expressed in classical Hodgkin lymphoma. J Pathol. 2017;243:220–9. [PubMed: 28722111]
10. Siegel RL, Miller KD, Jemal A. Cancer statistics, 2017. CA: A Cancer J Clin. 2017;67:7–30.

11. Li J, Yen C, Liaw D, Podsypanina K, Bose S, Wang SI, et al. PTEN, a putative protein tyrosine phosphatase gene mutated in human brain, breast, and prostate cancer. Science. 1997;275:1943–7. [PubMed: 9072974]
12. Chalhoub N, Baker SJ. PTEN and the PI3-kinase pathway in cancer. Annu Rev Pathol. 2009;4:127–50. [PubMed: 18767981]
13. Wu X, Wu J, Huang J, Powell WC, Zhang J, Matusik RJ, et al. Generation of a prostate epithelial cell-specific Cre transgenic mouse model for tissue-specific gene ablation. Mech Dev. 2001;101:61–9. [PubMed: 11231059]
14. Wang S, Gao J, Lei Q, Rozengurt N, Pritchard C, Jiao J, et al. Prostate-specific deletion of the murine Pten tumor suppressor gene leads to metastatic prostate cancer. Cancer Cell. 2003;4:209–21. [PubMed: 14522255]
15. Fu Y, Wey S, Wang M, Ye R, Liao CP, Roy-Burman P, et al. Pten null prostate tumorigenesis and AKT activation are blocked by targeted knockout of ER chaperone GRP78/BiP in prostate epithelium. Proc Natl Acad Sci USA. 2008;105:19444–9. [PubMed: 19033462]
16. Adisetiyo H, Liang M, Liao CP, Aycock-Williams A, Cohen MB, Xu S, et al. Loss of survivin in the prostate epithelium impedes carcinogenesis in a mouse model of prostate adenocarcinoma. PLoS ONE. 2013;8:e69484. [PubMed: 23936028]
17. Gottowik J, Cesura AM, Malherbe P, Lang G, Da Prada M. Characterisation of wild-type and mutant forms of human monoamine oxidase A and B expressed in a mammalian cell line. FEBS Lett. 1993;317:152–6. [PubMed: 8428624]
18. Ma J, Ito A. Tyrosine residues near the FAD binding site are critical for FAD binding and for the maintenance of the stable and active conformation of rat monoamine oxidase A. J Biochem. 2002;131:107–11. [PubMed: 11754741]
19. Bortolato M, Chen K, Godar SC, Chen G, Wu W, Rebrin I, et al. Social deficits and perseverative behaviors, but not overt aggression, in MAO-A hypomorphic mice. Neuropsychopharmacology. 2011;36:2674–88. [PubMed: 21832987]
20. Dillon LM, Miller TW. Therapeutic targeting of cancers with loss of PTEN function. Curr Drug Targets. 2014;15:65–79. [PubMed: 24387334]
21. Tuominen VJ, Ruotoistenmaki S, Viitanen A, Jumppanen M, Isola J. ImmunoRatio: a publicly available web application for quantitative image analysis of estrogen receptor (ER), progesterone receptor (PR), and Ki-67. Breast Cancer Res. 2010;12:R56. [PubMed: 20663194]
22. Dubrovska A, Kim S, Salamone RJ, Walker JR, Maira SM, Garcia-Echeverria C, et al. The role of PTEN/Akt/PI3K signaling in the maintenance and viability of prostate cancer stem-like cell populations. Proc Natl Acad Sci USA. 2009;106:268–73. [PubMed: 19116269]
23. Sahlberg SH, Spiegelberg D, Glimelius B, Stenerlow B, Nestor M. Evaluation of cancer stem cell markers CD133, CD44, CD24: association with AKT isoforms and radiation resistance in colon cancer cells. PLoS ONE. 2014;9:e94621. [PubMed: 24760019]
24. Dawood S, Austin L, Cristofanilli M. Cancer stem cells: implications for cancer therapy. Oncology (Williston Park). 2014;28:1101–7. [PubMed: 25510809]
25. Collins AT, Berry PA, Hyde C, Stower MJ, Maitland NJ. Prospective identification of tumorigenic prostate cancer stem cells. Cancer Res. 2005;65:10946–51. [PubMed: 16322242]
26. Al-Hajj M, Becker MW, Wicha M, Weissman I, Clarke MF. Therapeutic implications of cancer stem cells. Curr Opin Genet Dev. 2004;14:43–7. [PubMed: 15108804]
27. Tan BT, Park CY, Ailles LE, Weissman IL. The cancer stem cell hypothesis: a work in progress. Lab Investig. 2006;86:1203–7. [PubMed: 17075578]
28. van den Berg DL, Snoek T, Mullin NP, Yates A, Bezstarosti K, Demmers J, et al. An Oct4-centered protein interaction network in embryonic stem cells. Cell Stem Cell. 2010;6:369–81. [PubMed: 20362541]
29. Vlietstra RJ, van Alewijk DC, Hermans KG, van Steenbrugge GJ, Trapman J. Frequent inactivation of PTEN in prostate cancer cell lines and xenografts. Cancer Res. 1998;58:2720–3. [PubMed: 9661880]
30. Takubo K, Goda N, Yamada W, Iriuchishima H, Ikeda E, Kubota Y, et al. Regulation of the HIF-1alpha level is essential for hematopoietic stem cells. Cell Stem Cell. 2010;7:391–402. [PubMed: 20804974]

31. Forristal CE, Nowlan B, Jacobsen RN, Barbier V, Walkinshaw G, Walkley CR, et al. HIF-1alpha is required for hematopoietic stem cell mobilization and 4-prolyl hydroxylase inhibitors enhance mobilization by stabilizing HIF-1alpha. Leukemia. 2015;29:1366–78. [PubMed: 25578474]
32. Cerami E, Gao J, Dogrusoz U, Gross BE, Sumer SO, Aksoy BA, et al. The cBio cancer genomics portal: an open platform for exploring multidimensional cancer genomics data. Cancer Discov. 2012;2:401–4. [PubMed: 22588877]
33. Gao J, Aksoy BA, Dogrusoz U, Dresdner G, Gross B, Sumer SO, et al. Integrative analysis of complex cancer genomics and clinical profiles using the cBioPortal. Sci Signal. 2013;6:pl1. [PubMed: 23550210]
34. Epstein JI, Zelefsky MJ, Sjoberg DD, Nelson JB, Egevad L, Magi-Galluzzi C, et al. A contemporary prostate cancer grading system: a validated alternative to the Gleason score. Eur Urol. 2016;69:428–35. [PubMed: 26166626]
35. Oliveira DS, Dzinic S, Bonfil AI, Saliganan AD, Sheng S, Bonfil RD. The mouse prostate: a basic anatomical and histological guideline. Bosn J Basic Med Sci. 2016;16:8–13. [PubMed: 26773172]
36. Liao CP, Zhong C, Saribekyan G, Bading J, Park R, Conti PS, et al. Mouse models of prostate adenocarcinoma with the capacity to monitor spontaneous carcinogenesis by bioluminescence or fluorescence. Cancer Res. 2007;67:7525–33. [PubMed: 17671224]
37. Sun H, Lesche R, Li DM, Liliental J, Zhang H, Gao J, et al. PTEN modulates cell cycle progression and cell survival by regulating phosphatidylinositol 3,4,5,-trisphosphate and Akt/protein kinase B signaling pathway. Proc Natl Acad Sci USA. 1999;96:6199–204. [PubMed: 10339565]
38. Alimonti A, Carracedo A, Clohessy JG, Trotman LC, Nardella C, Egia A, et al. Subtle variations in Pten dose determine cancer susceptibility. Nat Genet. 2010;42:454–8. [PubMed: 20400965]
39. Gu G, Yuan J, Wills M, Kasper S. Prostate cancer cells with stem cell characteristics reconstitute the original human tumor in vivo. Cancer Res. 2007;67:4807–15. [PubMed: 17510410]
40. Lawson DA, Xin L, Lukacs R, Xu Q, Cheng D, Witte ON. Prostate stem cells and prostate cancer. Cold Spring Harb Symp Quant Biol. 2005;70:187–96. [PubMed: 16869753]
41. Nikitin AY, Matoso A, Roy-Burman P. Prostate stem cells and cancer. Histol Histopathol. 2007;22:1043–9. [PubMed: 17523082]
42. Pfeiffer MJ, Schalken JA. Stem cell characteristics in prostate cancer cell lines. Eur Urol. 2010;57:246–54. [PubMed: 19200636]
43. Liao CP, Adisetiyo H, Liang M, Roy-Burman P. Cancer-associated fibroblasts enhance the gland-forming capability of prostate cancer stem cells. Cancer Res. 2010;70:7294–303. [PubMed: 20807814]
44. Liao CP, Adisetiyo H, Liang M, Roy-Burman P. Cancer stem cells and microenvironment in prostate cancer progression. Horm Cancer. 2010;1:297–305. [PubMed: 21761361]
45. Adisetiyo H, Liang M, Liao CP, Jeong JH, Cohen MB, Roy-Burman P, et al. Dependence of castration-resistant prostate cancer (CRPC) stem cells on CRPC-associated fibroblasts. J Cell Physiol. 2014;229:1170–6. [PubMed: 24752784]
46. Ting MC, Liao CP, Yan C, Jia L, Groshen S, Frenkel B, et al. An enhancer from the 8q24 prostate cancer risk region is sufficient to direct reporter gene expression to a subset of prostate stem-like epithelial cells in transgenic mice. Dis Models Mech. 2012;5:366–74.
47. Goldstein AS, Huang J, Guo C, Garraway IP, Witte ON. Identification of a cell of origin for human prostate cancer. Science. 2010;329:568–71. [PubMed: 20671189]
48. Leong KG, Wang BE, Johnson L, Gao WQ. Generation of a prostate from a single adult stem cell. Nature. 2008;456:804–8. [PubMed: 18946470]
49. Xu S, Adisetiyo H, Tamura S, Grande F, Garofalo A, Roy-Burman P, et al. Dual inhibition of survivin and MAOA syner-gistically impairs growth of PTEN-negative prostate cancer. British Journal of Cancer. 2015;113:242–51. [PubMed: 26103574]
50. The Cancer Genome Atlas Research Network. The molecular taxonomy of primary prostate cancer. Cell. 2015;163:1011–25.. [PubMed: 26544944]

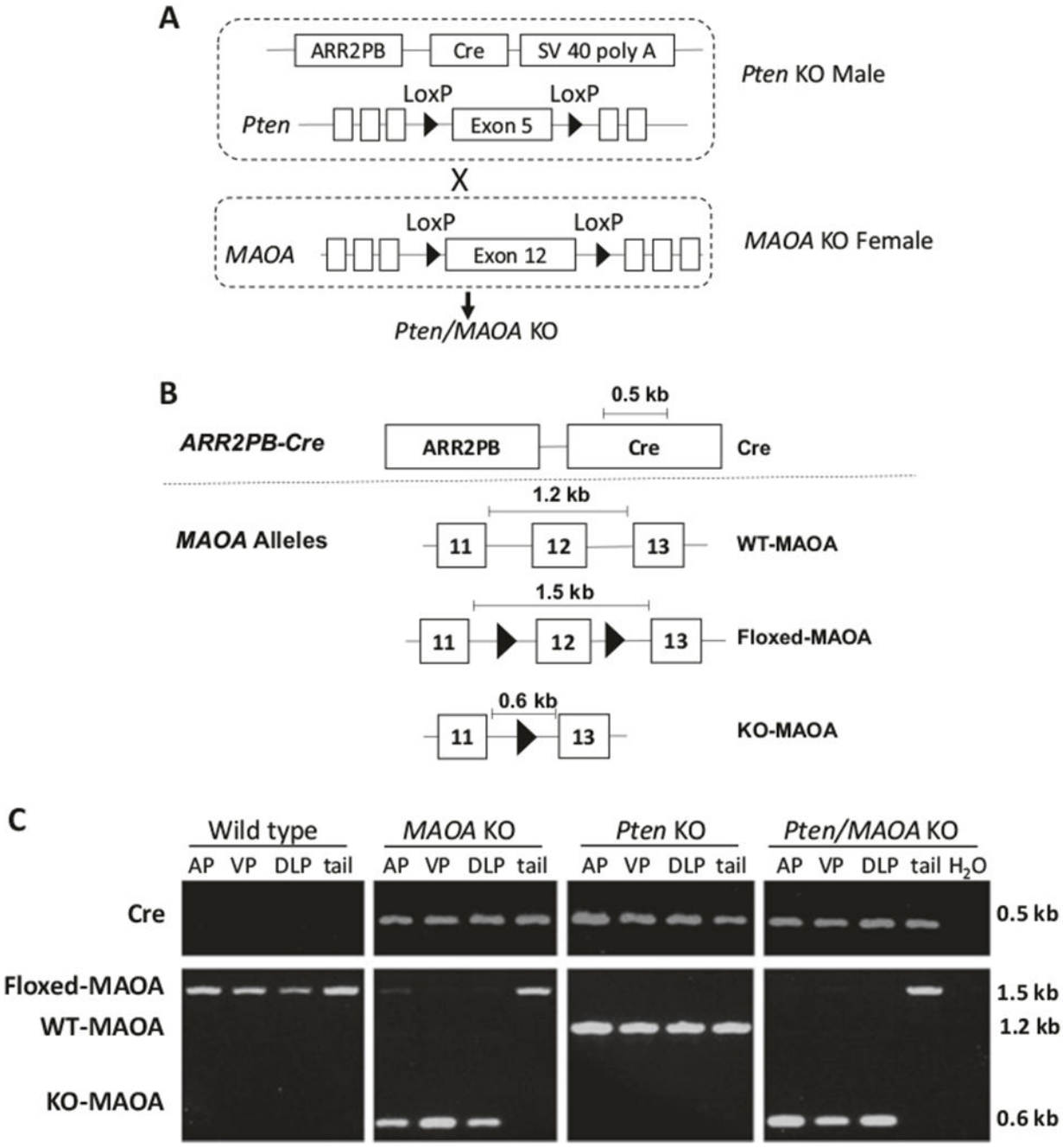

Fig. 1.

Generation of *MAOA* KO and *Pten/MAOA* KO mice. **a** *Pten/MAOA* KO mice were generated by crossing male *Pten* KO mice carrying *Cre* transgene and floxed *Pten* exon 5, with female *MAOA* KO mice carrying floxed-*MAOA* exon 12, which comprises the covalent FAD-binding site. **b** Schematic representation for ARR2PB-*Cre* and *MAOA* alleles. **c** Genotypes of mice were determined by PCR of genomic DNA isolated from both prostate and tail tissues. Upper: a 0.5-kb band represented the *Cre* gene in *MAOA* KO, *Pten* KO, and *Pten/MAOA* KO mice. Lower: the intact loxP-*MAOA* gene (1.5-kb band) was detected in

the prostate and the tail of wild type and only in the tails of other three genotypes. The wild-type *MAOA* gene (1.2-kb band) was only detected in *Pten* KO. Finally, the *MAOA* recombinant (0.6-kb band) was detected in prostate in *MAOA* KO, *Pten* KO, and *Pten/MAOA* KO mice

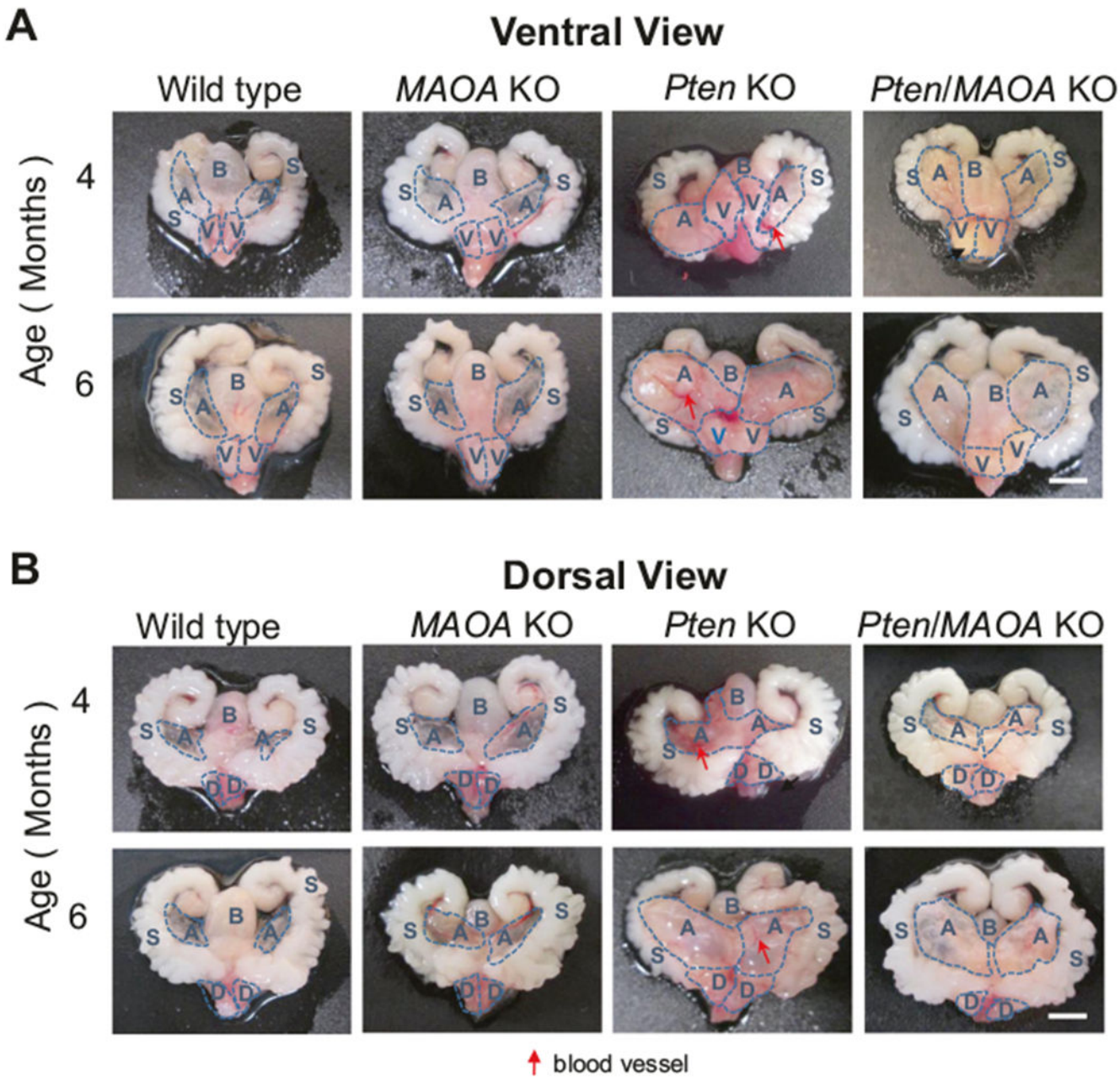

Fig. 2.

MAOA deletion attenuated the cancer morphology in *Pten/MAOA* KO prostates. Images of intact prostates dissected from all four genotypes at 4 and 6 months old were presented. **a** Ventral view. **b** Dorsal view. Prostate lobes were circled with dashed lines and marked. *A* anterior prostate, *V* ventral prostate, *D* dorsal–lateral prostate, *B* bladder, *S* seminal vesicle. Bar, 5 mm. Red arrow: blood vessels

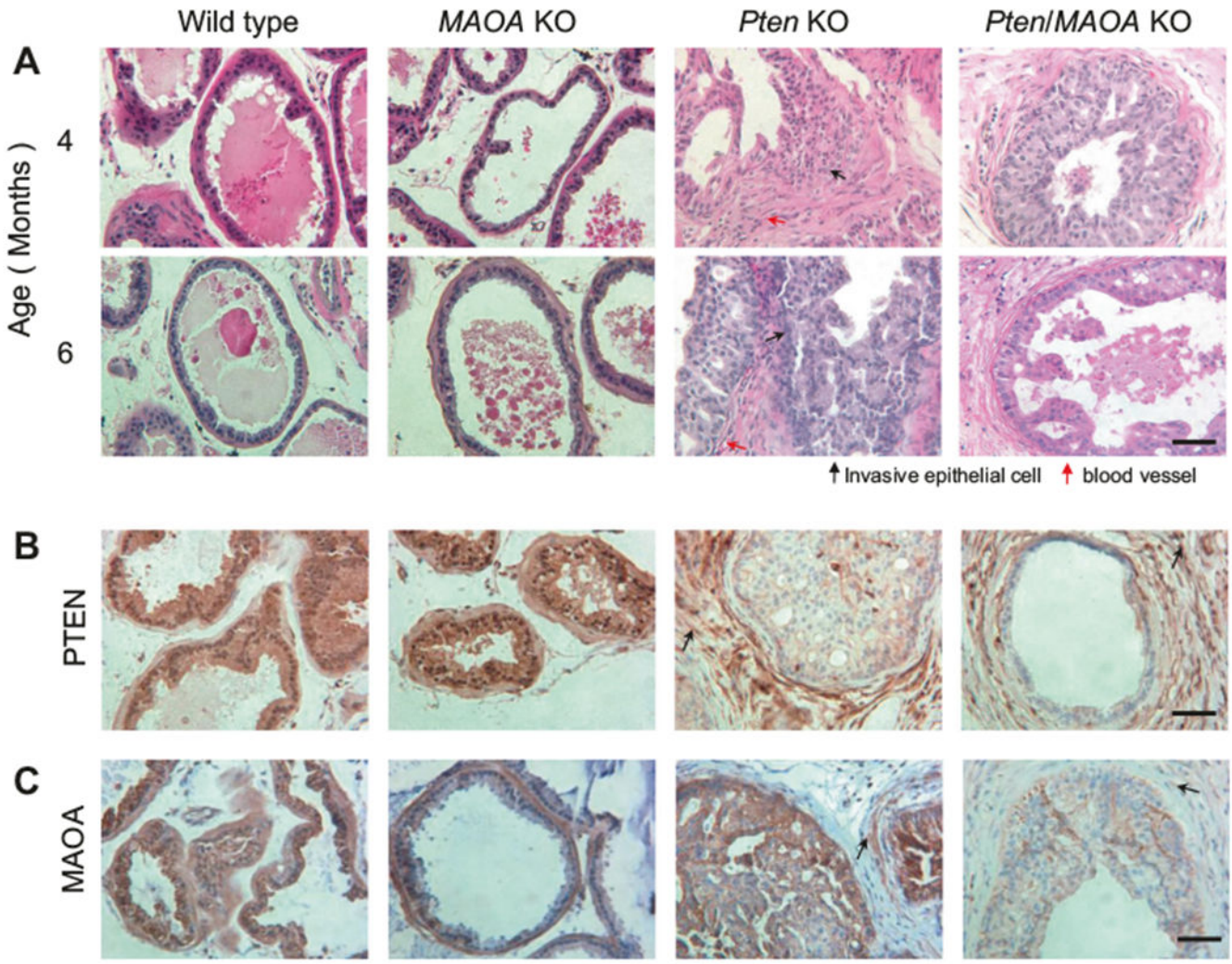

Fig. 3.

Histologic analysis of murine prostatic tissue sections. **a** H&E staining of paraffin-embedded DLP tissue sections dissected from all four genotypes at 4 and 6 months of age. Bar, 50 μm. Black arrow: invasive epithelial cells; red arrow: blood vessels. **b**, **c** The expression of PTEN (**b**) and MAOA (**c**) detected by IHC in 6-month-old DLP lobes of four genotypes (wild type, *MAOA* KO, *Pten* KO, and *Pten/MAOA* KO). Arrow: positive cells. Bar, 50 μm

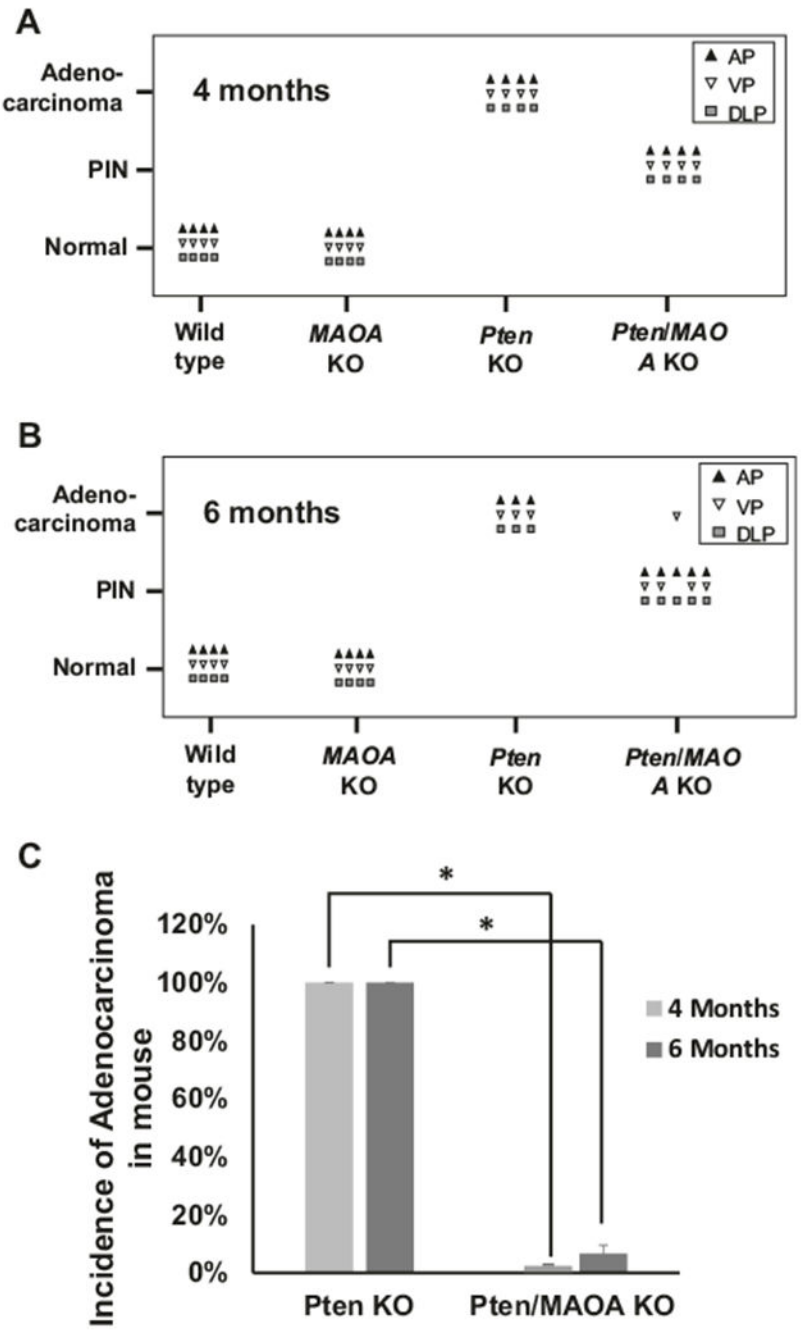

Fig. 4.

The distribution of three histological states, normal, PIN, and adenocarcinoma, in prostate lobes in each genotype at (**a**) 4 months and (**b**) 6 months of age. ▲: AP; ▽: VP; ■: DLP. n = 4 in each group, except in **b** *Pten/MAOA* KO, n = 5. *Pten* KO showed the presence of adenocarcinoma in all 4 mice in all prostate lobes (AP, VP, and DLP) at both 4 and 6 months of age. *Pten/MAOA* KO mice show PIN in all 4 mice in all prostate lobes at 4 months. Similar finding was observed in 6 months, except 1 mouse in VP showed adenocarcinoma

out of 5 mice. **c** The incidence of adenocarcinoma in mouse from *Pten* KO and *Pten/MAOA* KO were compared. Data represent the mean ± SEM, $*p < 0.01$

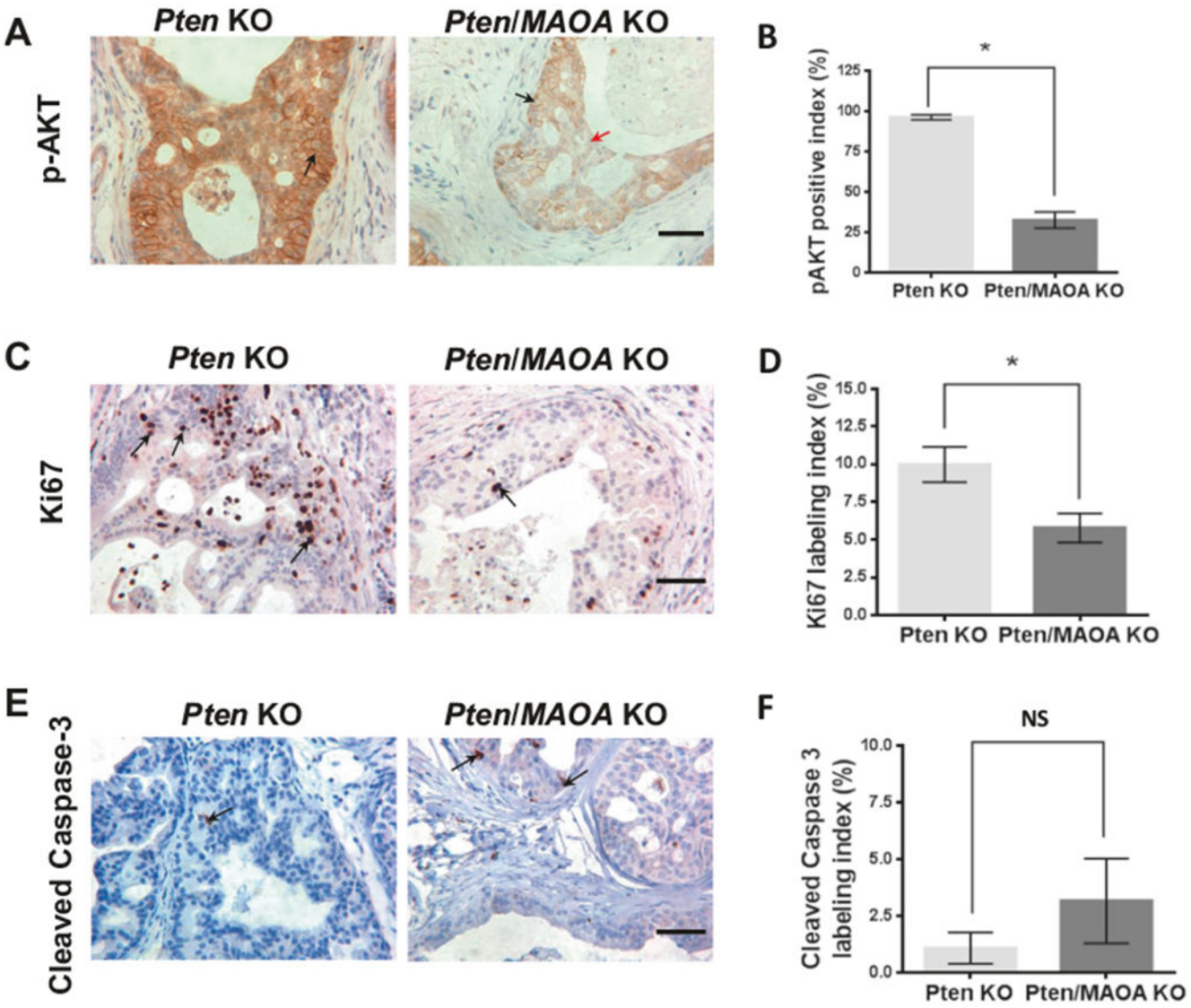

Fig. 5.

MAOA deletion in PCa suppressed AKT activity and cell proliferation but induced apoptosis in *Pten/MAOA* KO mice. IHC staining was performed on 6-month-old DLP sections collected from *Pten* KO and *Pten/MAOA* KO. **a**, **c** p-AKT-positive cells and proliferating prostate cells were identified by p-AKT (**a**) and Ki67 (**c**) antibodies, respectively. Black arrow: positive epithelial cell; red arrow: negative epithelial cell. Bar, 50 μm. **e** Detections of apoptotic cells by cleaved caspase-3 staining. Black arrow: cleaved caspase-3-positive epithelial cells. Bar, 50 μm. **b**, **d**, **f** Comparing the percentage of positive staining cells in epithelium between two genotypes. *$p < 0.05$. *NS* not significant

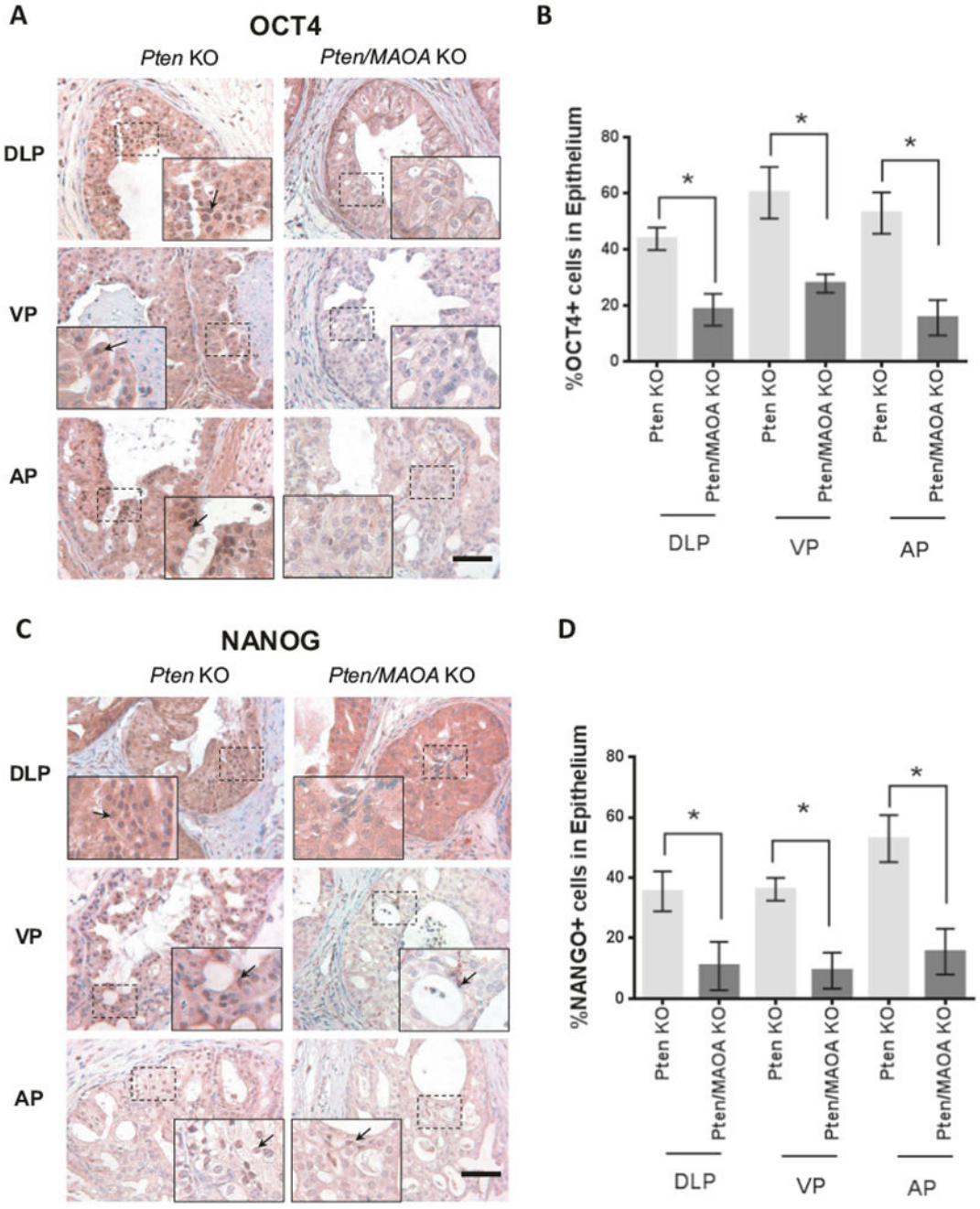

Fig. 6.

MAOA deletion reduced cancer stem cell populations in epithelium in *Pten/MAOA* KO. **a**, **c** IHC images of (**a**) OCT4 and (**c**) NANOG staining on DLP, AP, and VP sections collected from 6-month-old *Pten* KO and DKO mice. Positive cells were detectable with nucleus staining. Black arrow: positive cells. Bar, 50 μm. **b**, **d** The quantitation of OCT4- and Nanog-positive stained epithelial cell in different prostate lobes in *Pten/MAOA* KO and *Pten KO* mice. Data represent the mean ± SD. *$p < 0.05$

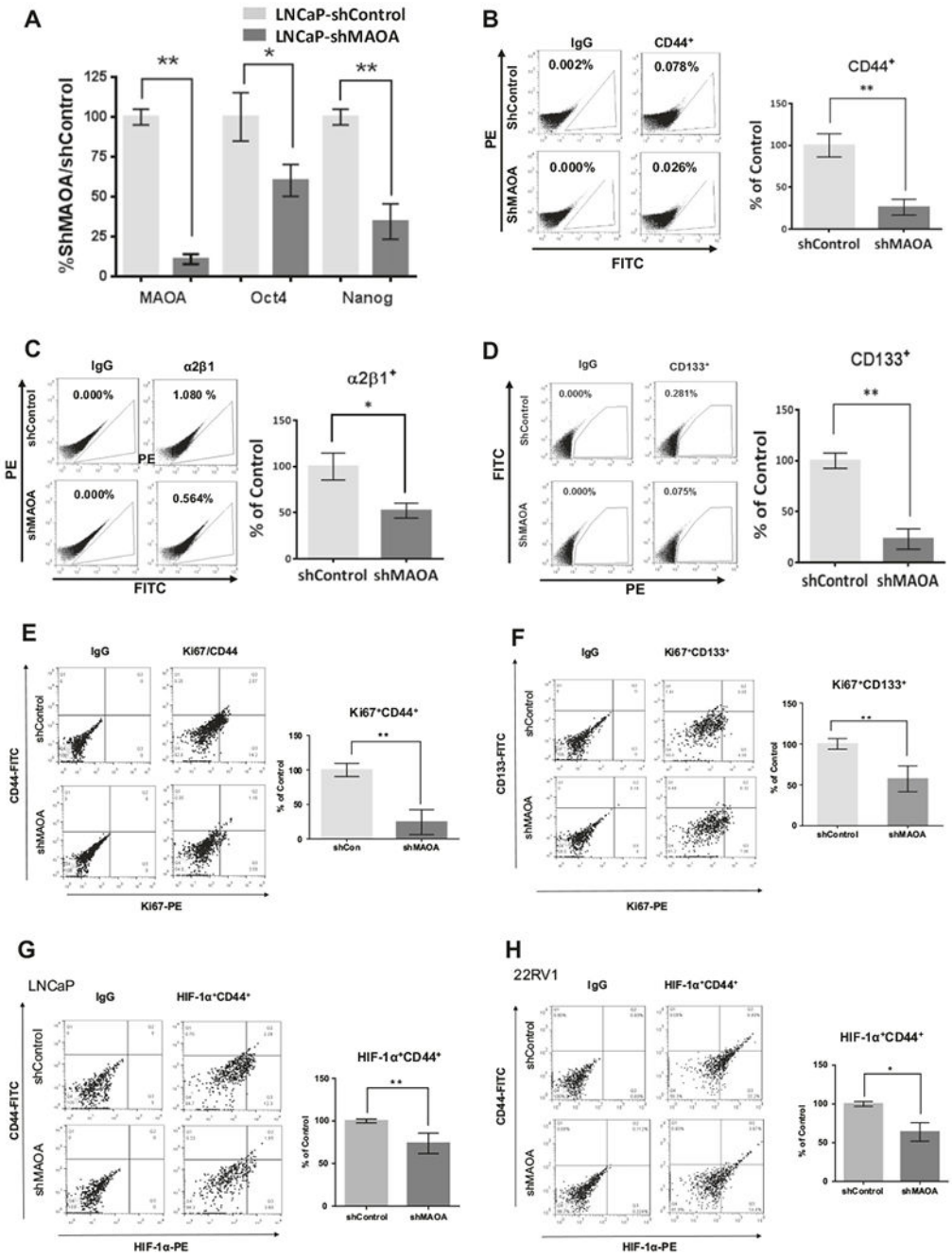

Fig. 7.

shMAOA PCa cell lines showed reduced stemness populations and cancer cell proliferation. **a** Reduced mRNA levels of *Oct4* and *Nanog* in LNCaP-shMAOA compared to LNCaP-shControl. mRNA levels were determined by RT-PCR. **b–d** CD44 (**b**)-, α2β1 (**c**)-, and CD133 (**d**)-positive stem cell populations in LNCaP-shMAOA and -shControl cells determined by flow cytometry. Each panel includes both gating plot and quantification of positive cells in shMAOA and shControl cells. These experiments were performed at least three times. **e**, **f** Comparing proliferative stemness cell populations in LNCaP: $Ki67^{+}CD44^{+}$

cells (**e**) and $Ki67^{+}CD133^{+}$ cells (**f**). **g**, **h** Detection of $HIF\text{-}1\alpha^{+}CD44^{+}$ stem cell populations in shMAOA as compared to shControl under hypoxia condition: LNCaP (**g**) and 22RV1 (**h**). Data represent the mean ± SD. $*p < 0.05$, $**p < 0.01$

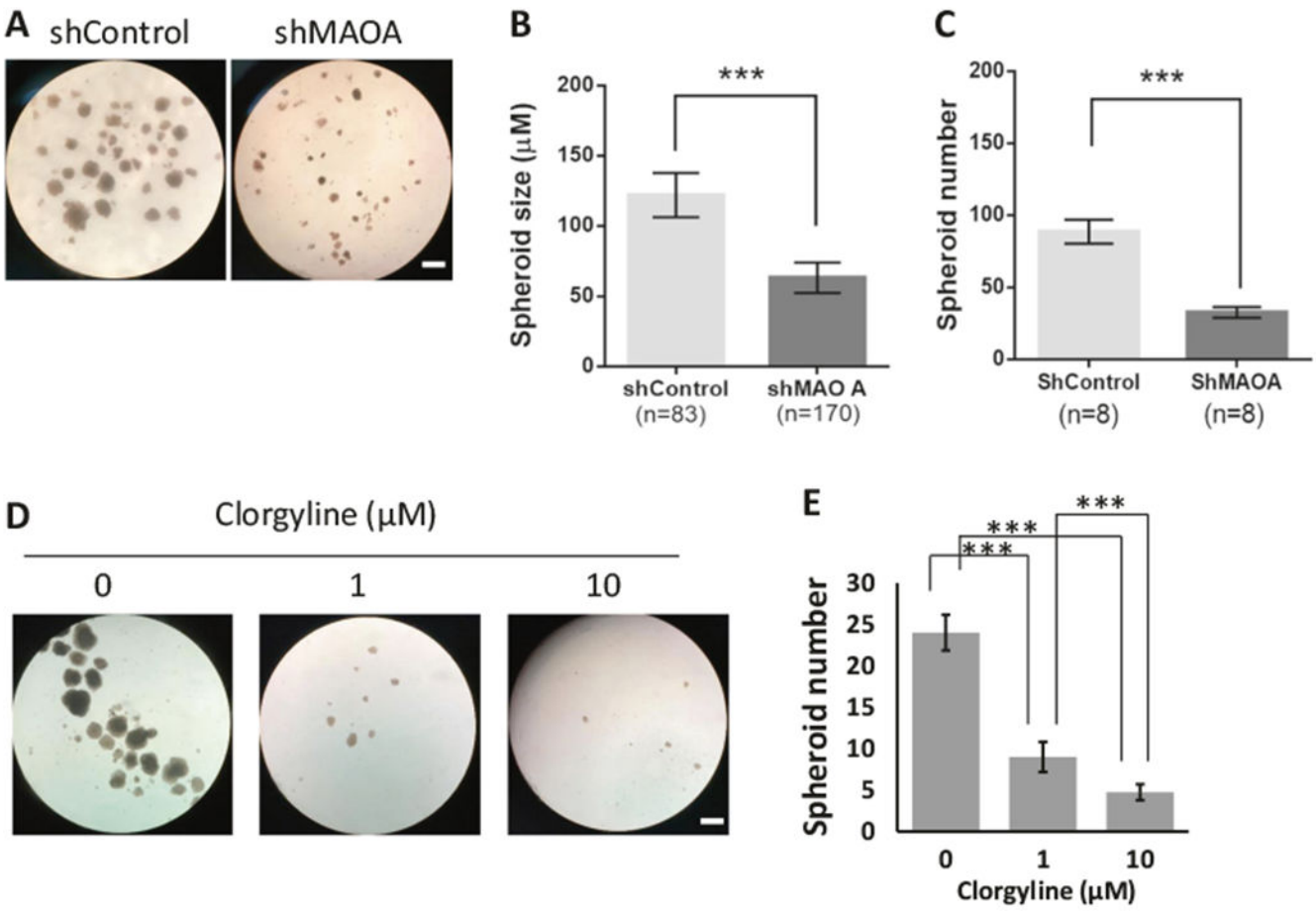

Fig. 8.

Loss of MAOA reduced the size of spheroid formed in 3D Matrigel cultures. **a** Representative bright-field images of spheroids formed from transformed LNCaP or 22RV1 (shControl or shMAOA) cells after 12 days of culture in 3D Matrigel. Bar, 100 μm. **b**, **c** Comparing the size (in diameter) (**b**) and number (**c**) of spheroid formed from two LNCaP cell lines. ***$p < 0.001$. **d** Representative images of spheroid forming of LNCaP cells with clorgyline treatments. Bar, 100 μm. **e** Comparing the number of LNCaP spheroid formed at different clorgyline concentrations. ***$p < 0.001$

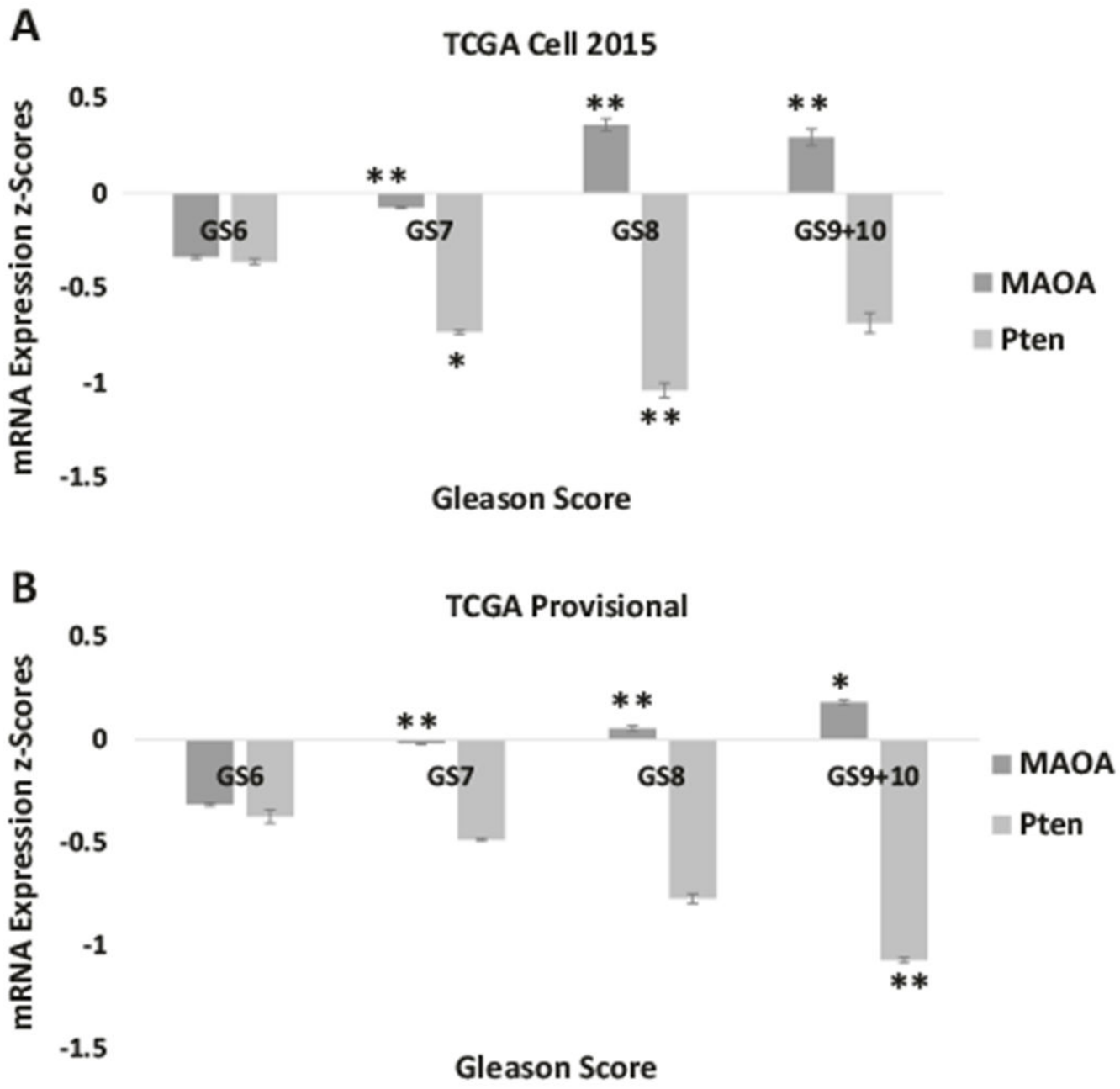

Fig. 9.

Patients with Gleason score 7 and above showed increase MAOA and decrease *Pten* expression. Two TCGA datasets with clinical annotation, including Gleason scores were used to interrogate the RNA expression of MAOA and *Pten*: **a** 236 patients from the dataset published in [50]; and **b** 491 patients from unpublished provisional PCa dataset [32, 33]. Data represent the mean ± SEM. *$p < 0.05$, **$p < 0.01$

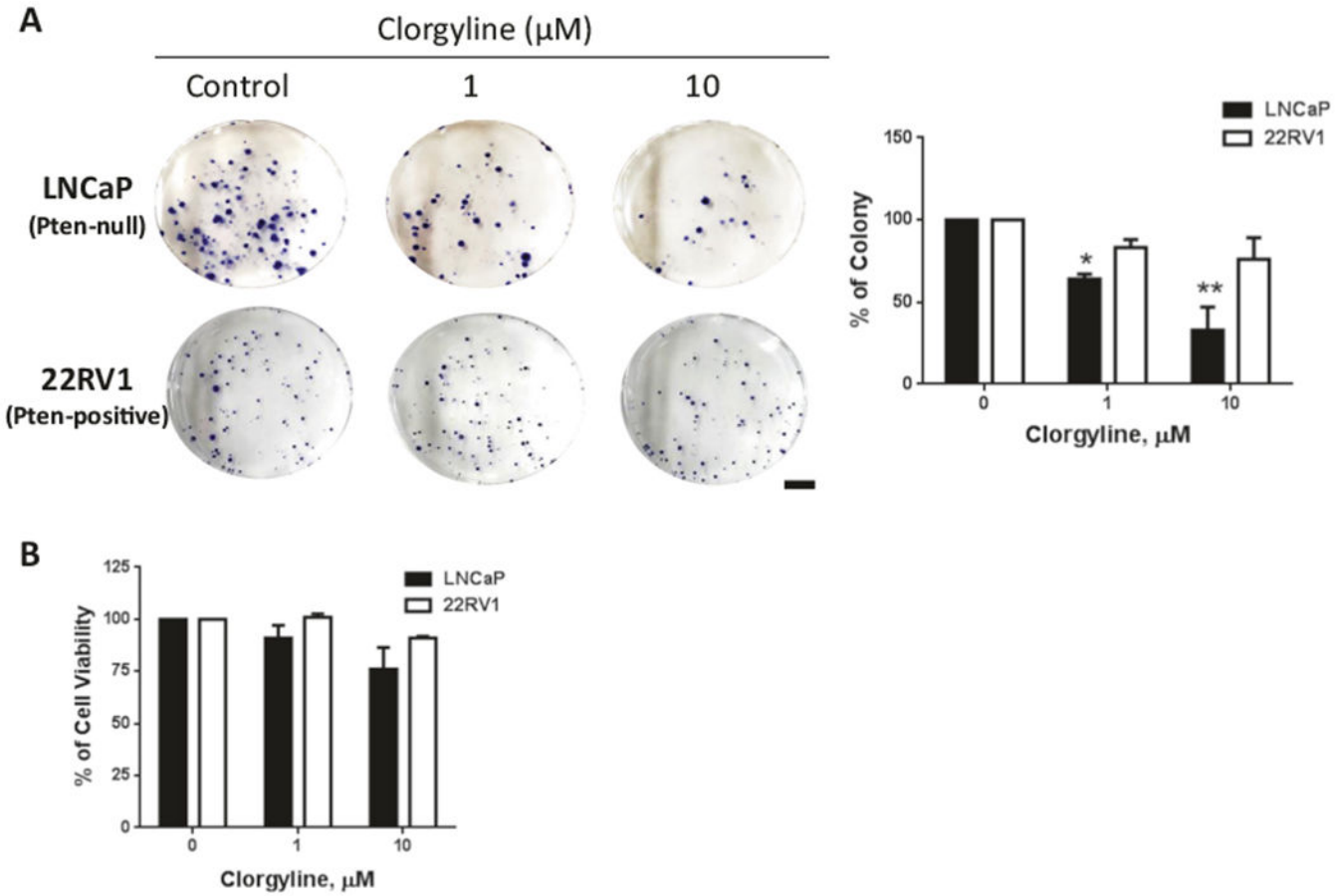

Fig. 10.

Clorgyline inhibitions in tumorigenesis and sternness were associated with *Pten* status in PCa cells. Comparing clorgyline treatments using PCa cells with *Pten*-null and -positive expressions. **a** 2D colony cultures of LNCaP (*Pten*-null) and 22RV1(*Pten*-positive) cells under treatments. Colonies were counted and compared (normalized by untreated controls). **b** Comparing cell viability of LNCaP and 22RV1 in MTT assay under treatments (normalized by untreated controls). Data represent the mean ± SD. *$p < 0.05$, **$p < 0.01$

Table 1

Primers and PCR conditions used for genotyping

Gene	Direction	Sequence (5′–3′)	Size of PCR product (bp)
Cre	Forward	GATCCTGGCAATTTCGGCTAT	500
	Reverse	TTGCCTGCATTACCGGTCGAT	
Pten	Forward	AAGCAAGCACTCTGCGAAACTGA	WT = 500; Floxed =670
	Reverse	GATTGTCATCTTCACTTAGCCATTGGT	
MAOA	Forward	GAATGAGAGTATCCTCTCTTCC	WT = 1200; Floxed = 1500; KO = 600
	Reverse	GTGGGATACTATATCCTATGTCTG	